Nanoscale

Accepted Manuscript

This is an *Accepted Manuscript*, which has been through the RSC Publishing peer review process and has been accepted for publication.

Accepted Manuscripts are published online shortly after acceptance, which is prior to technical editing, formatting and proof reading. This free service from RSC Publishing allows authors to make their results available to the community, in citable form, before publication of the edited article. This *Accepted Manuscript* will be replaced by the edited and formatted *Advance Article* as soon as this is available.

To cite this manuscript please use its permanent Digital Object Identifier (DOI®), which is identical for all formats of publication.

More information about *Accepted Manuscripts* can be found in the **Information for Authors**.

Please note that technical editing may introduce minor changes to the text and/or graphics contained in the manuscript submitted by the author(s) which may alter content, and that the standard **Terms & Conditions** and the **ethical guidelines** that apply to the journal are still applicable. In no event shall the RSC be held responsible for any errors or omissions in these *Accepted Manuscript* manuscripts or any consequences arising from the use of any information contained in them.

Improved thermal stability of oxide-supported naked gold nanoparticles by ligand-assisted pinning

César Moreno,*[a] Núria J. Divins,[a,b] Jaume Gázquez,[c,d] Maria Varela,[d,c] Inmaculada Angurell,[e] and Jordi Llorca[a,b]

Received Xth XXXXXXXXXX 20XX, Accepted Xth XXXXXXXXX 20XX

First published on the web Xth XXXXXXXXXX 200X

DOI: 10.1039/b000000x

We report a method to improve thermal stability up to $900\,^{\circ}C$ of bare-metal (naked) nanoparticles of gold supported on top of SiO_2 and $SrTiO_3$ substrates via ligand-assisted pinning. This approach leads to monodisperse naked gold nanoparticles without significant sintering after thermal annealing in air at $900\,^{\circ}C$. The ligand-assisted pinning mechanism is described.

Electromagnetic, optical and catalytic properties of metal nanoparticles are strongly sensitive to the shape and size.[1] A conventional technique to synthesize nanoparticles (NPs) presenting controlled shape and size is the use of stabilizing agents or ligands.[2] The application of these nanoparticles requires the removal of ligands which prevent the extremely high tendency of adhesion and aggregation to the detriment of nanoparticle functionality which are governed mainly by the particle cores. Very often thermal annealing for stripping away the organic ligand shell is used, involving changes in nanoparticle size and shape and therefore a deterioration of their functional properties.[3,4] Furthermore, thermal stability up to elevated temperatures is not only highly desirable for the nanoparticle community as a strategy to remove ligands, but also in order to use NPs in real world applications as catalysis, photonics, bio-sensors or biomedical drug delivery.[5–8] Focusing in catalysis applications, oxide-supported gold nanoparticles catalysts are considered as a promising system.[4,9,10] A critical issue is the catalytic activity drop caused by sintering of Au nanoparticles at high temperature involving a decrease of the specific surface area and, consequently, the degradation of the catalytic activity. Thus, when gold nanoparticles have a diameter below 10 nm, it leads to boosted catalytic activity.[9] Many approaches have been attempted to avoid the aggregation of the nanoparticles as alloying, encapsulation and etching, surface treatment or by using reducible supports (i.e. TiO_2, ZrO_2 or CeO_2) exhibiting a strong metal-support interaction.[10–15] However, it is still a challenging issue to stabilize naked gold nanoparticles in a non-reducible supports as silica (SiO_2) due to the weak metal-support interaction, as compared to reducible supports, and therefore displaying a low temperature of sintering at $200-400\,^{\circ}C$. But silica support have been attracting growing interest from the point of view thermal stability, chemical inertness and stability in acidic environments. Recently, it has been reported surprising thermal stability of Au/SiO_2 up to at least $500\,^{\circ}C$ attributed to impurities and defects of silica surface[3] and up to $700\,^{\circ}C$ for a Au/TiO_2 system decorated by amorphous SiO_2[16] mainly attributed to the high thermal stability of the SiO_2 component.[17]

In this work we present an alternative approach for stabilizing naked gold nanoparticles, with a particle diameters below 10 nm, supported on SiO_2 and $SrTiO_3$, based in the use of Si-rich trimethyl silane (TMS) ligand shell to control the interparticle distance that reduces sintering up to at least $900\,^{\circ}C$, and immobilizes the particles remaining in the same position after stepwise annealing treatments.

Core-shell gold nanoparticles with TMS ligands (Au@TMS) were synthesized with $HS(CH_2)_3SiMe_3$ as previously reported.[18] Au@TMS were deposited by dip-coating onto thermally oxidized silicon wafer provided with a SiO_2 surface layer and onto $SrTiO_3$ (STO) single crystal and annealed during 30 minutes at different temperatures in a conventional furnace in air atmosphere. X-ray photoelectron spectra (XPS) were recorded at a pressure below 10^{-9} mbar with a SPECS system. All binding energy values were refered to Ti(2p) peak at 457.9 eV.[19] Topographic scanning force microscopy (SFM) images were performed using a Veeco Dimension microscope operated at ambient conditions in dynamic mode with the same tip for all measurements. For scanning transmission electron microscopy-electron energy loss spectroscopy (STEM-EELS) a VG HB501UX Microscope was used, operated at 100 kV and equipped with a Nion aberration corrector and an Enfina Gatan spectrometer. Specimens were prepared by conventional thinning, grinding

[a] *Centre de Recerca en Nanoenginyeria, UPC, Barcelona 08028, Spain. E-mail: cesar.moreno.sierrra@upc.edu*

[b] *Institut de Tècniques Energètiques,UPC, Barcelona 08028, Spain.*

[c] *Departamento de Física Aplicada III, UCM, Madrid 28040 Spain.*

[d] *Materials Science and Technology Division, ORNL, Oak Ridge, Tennessee 32831, USA.*

[e] *Departament de Química Inorgànica, UB, Barcelona 08028, Spain.*

and Ar ion milling.

Figure 1(a-e) displays typical topographic images of the supported Au@TMS deposited onto SiO_2 at different annealing temperatures. After a low temperature annealing (80 °C) (a) a cellular network structure is formed. In order to remove the ligand shell we performed recurrent annealing at 450 °C, 550 °C and 700 °C (b-d). By increasing the annealing temperature up to 900 °C (e) the TMS ligands were progressively removed displaying Au NPs. In this step, 94.7% are monodisperse nanoparticles with an average height 2-3 nm (Fig.1(e,f)) free from TMS ligand residues while a marginal 5.3% of the NPs changed the size (4-30 nm). This is in accordance with the range of 2-3 nm of diameter determined by high resolution transmission electron microscopy (HRTEM) previously reported for the Au cores in the as synthesized Au@TMS.[18] In the inset of figure 1(e) we display the phase image where the position of Au NPs (dark contrast) is more easily identified. Notice that the same cellular network structure of the initial stage remains after annealing at 900 °C.

Similar behavior to Au@TMS onto SiO_2 is found when they are deposited onto STO single crystal substrate. After annealing at 900 °C the NPs are free of the TMS ligand shell presenting a monodisperse distribution of nanoparticles (Fig.1(g)) with sizes around 5-7 nm (Fig.1(h)). Comparing with the widely used Au-dodecanothiol NPs deposited on the same substrate, after annealing at (80 °C) Au-dodecanothiol NPs show similar distribution (Fig.1(i)) and after 450 °C the shell is removed and the nanoparticles are strongly sintered (Fig.1(j)). Figure 1(k) displays the Au NP average height as a function of annealing temperature obtained from the topographic images where error arises from the observed statistical distribution. This plot indicates that the average Au@TMS height is nearly constant up to 550 °C, while a slight decrease can be seen after removing the TMS ligand shell at 700 – 900 °C. However, a clear increase is observed in the case of the Au-dodecanothiol NPs, where strong sintering is produced in well agreement with the low Tammann temperature for gold (395 °C), which is the temperature at which the particles begin to sinter significantly.

In order to address the chemical environment of the Au NPs capped with a Si-rich TMS ligand we have performed XPS analysis on Au@TMS deposited onto STO substrate. Figure 2(a) shows the Si(2p) core level signal for the sample annealed at 80 °C which is ascribed to the Si-rich TMS ligand. In contrast, after annealing at 900 °C, an additional peak is displayed at higher binding energies (102.9 eV), indicating the presence of SiO_2.[20]

The surface C/Ti atomic ratio increased from 3.2 (ambient contamination) to 6.6 times after deposition of Au@TMS and decreased to 3.3 times after anneling at 900 °C. This means that most of the ligand carbon was removed from the Au@TMS. The Si/Ti atomic ratio decreased slightly (1.6 times) after annealing at 900 °C with respect to 80 °C due to the transformation and agglomeration of silicon from the TMS ligand to SiO_2. After annealing at 900 °C, the Au surface concentration measured decreased slightly. Taking into account that the size of the Au NPs almost remain constant after annealing, this could be related to a matrix effect (the source region of the electrons ejected by X-rays is different before and after removal of the TMS ligand) or as losses of melted gold at lower temperatures than that corresponding to the Au bulk.[21]

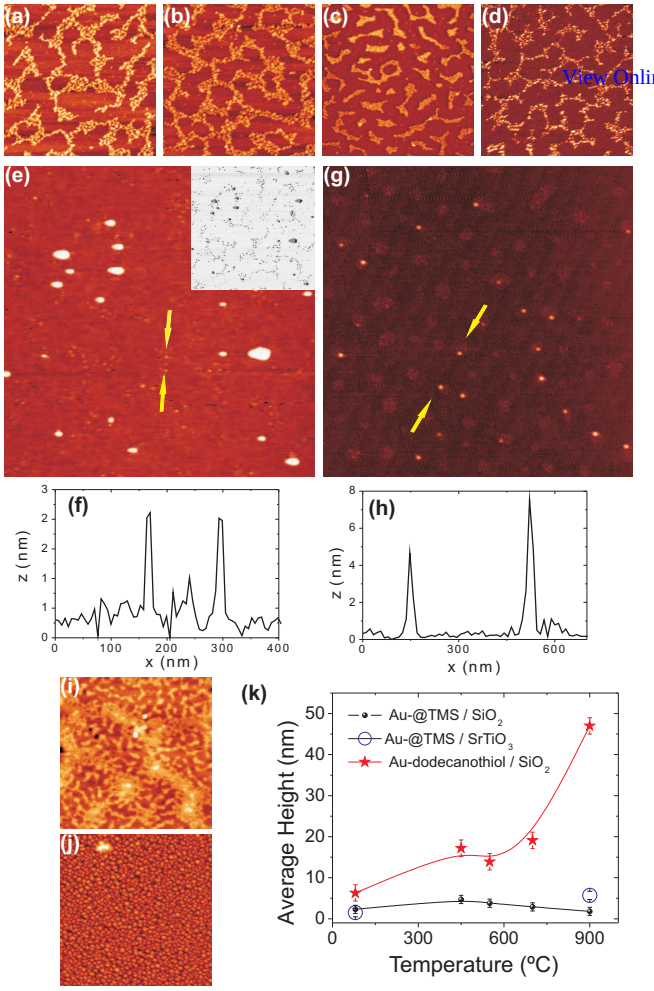

Fig. 1 Topographic SFM images ($3 \times 3 \mu m^2$) of supported Au NPs systems. Au@TMS on top of SiO_2 substrate after annealing at: (a) 80 °C, (b) 450 °C , (c) 550 °C, (d) 700 °C and (e) 900 °C. (f) Profile in (e) between arrows. Inset in (e) display the phase image.(g) Au@TMS on top of STO substrate after annelaing at 900 °C. (h) Profile in (g) between arrows. (i) Au-dodecanothiol on top of SiO_2 substrate after annealing at 80 °C and (j) after 450 °C. (k) Temperature dependence average height obtained from topographic images.

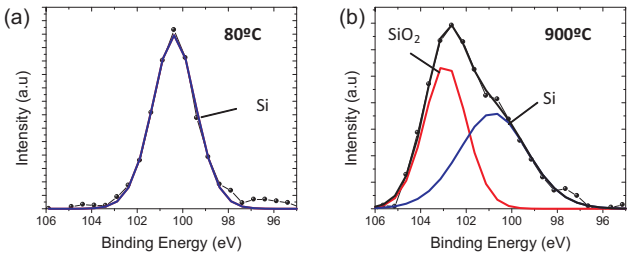

Fig. 2 Si 2p core-level spectra of Au@TMS onto STO after: (a) annealing at 80 °*C* and (b) 900 °*C*.

Figure 3(a) shows a low magnification annular dark-field (ADF) Z-contrast image of an Au small nanoparticle adjacent to a sintered Au NP laying onto the pristine amorphous SiO_2 layer that covers the thermally oxidized silicon wafer. The contrast in Z-contrast images is roughly proportional to the atomic number, so the heavier Au nanoparticle appears much brighter.

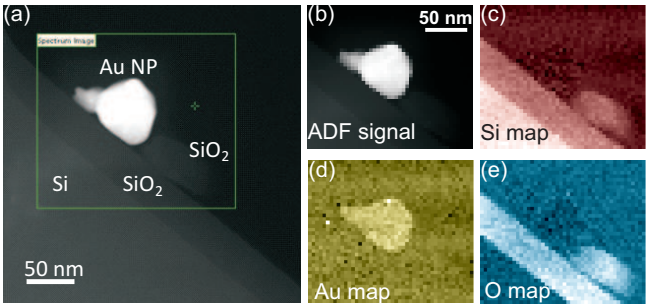

Fig. 3 Spectrum image of a Au nanoparticle after annealing at 900 °*C* laying on the Si substrate. (a) Low resolution ADF image. The square marks the area where the spectrum image was acquired. (b) ADF signal acquired simultaneously with the spectrum image. The nominal acquisition time was 0.1 s per pixel. (c, d) and (e) are the elemental maps for Si K edge around 1840 eV, Au $M_{4,5}$ edge around 2200 eV and O K edge around 530 eV, respectively.

The box in figure 3(a) shows the spectrum image region, with figure 3(b) being the simultaneously acquired ADF signal. For spectrum imaging, the electron beam is scanned along the image region and in every pixel an EEL spectrum is acquired, along with the ADF signal. Elemental mapping is then possible through a background subtraction and integration of the intensity remaining under the absorption edge. This way, Si, Au and O maps were obtained, figure 3(c,d) and (e) respectively, which allowed us to identify the feature next to the Au nanoparticle as SiO_2, which is in firm agreement with XPS data. Figure 4 illustrates the ligand-assisted pinning mechanism of oxide-supported nanoparticles. Gold nanoparticles functionalized with Si-rich ligand were deposited onto oxide substrates and upon high-temperature annealing, the Au@TMS did not form Au@SiO_2 core-shell structure, but formed Au-SiO_2 portrayed by SiO_2 sitting adjacent to gold nanoparticles, thus avoiding the sintering of naked gold nanoparticles.

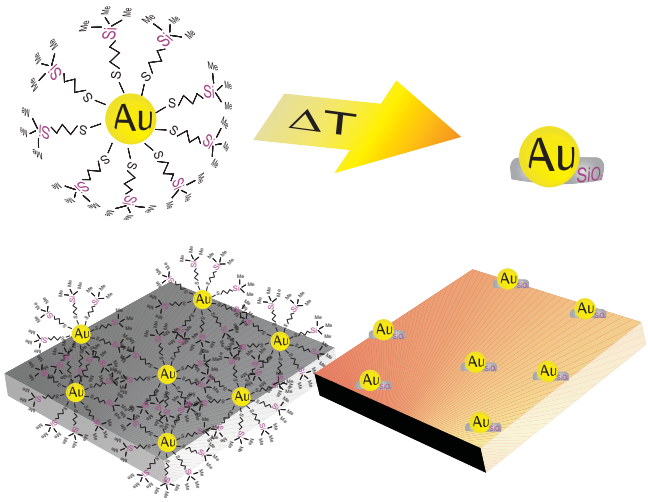

Fig. 4 Conceptual scheme of ligand-assisted pinnig mechanism for Au@TMS system.

In conclusion, outstanding thermal stability up to 900 °*C* has been demonstrated for small Au NPs in the range of 2-3 nm and 5-7 nm supported either on SiO_2 or STO substrates, respectively. XPS and STEM data show that, upon thermal annealing in air, the silicon which was initially around the core NP is progressively converted into SiO_2. The outcropped SiO_2 acts as a pinning center for the resulting Au NPs. This result opens the possibility to use gold nanoparticles to develop new potential applications operating at high temperatures.

Acknowledgements

Financial support from MICINN projects CTQ2009-08795 and CTQ2009-12520 and MSE Division DoE grant FG02-09ER46554 is acknowledged. J.L. is grateful to ICREA Academia program, J. G. to ERC Starting Investigator Award, grant 239739 STEMOX and N.J.D and C.M to UPC grants. Research at ORNL supported by the Materials Sciences and Engineering Division of the U.S. Department of Energy (MV). We would like to thank T. Puig and X. Obradors for kindly providing us with the STO substrates and J.Puigdollers for Si substrates.

References

1 Y. Song, Z. Zhang, H. E. Elsayed-Ali, H. Wang, L. L. Henry, Q. Wang, S. Zou and T. Zhang, *Nanoscale*, 2011, **3**, 31–44.

2 D. Astruc, E. Boisselier and C. Ornelas, *Chem. Rev.*, 2010, **110**, 1857–1959.
3 G. M. Veith, A. R. Lupini, S. Rashkeev, S. J. Pennycook, D. R. Mullins, V. Schwartz, C. A. Bridges and N. J. Dudney, *J. Catal.*, 2009, **262**, 92–101.
4 M. Haruta, *Chem. Rec.*, 2003, **3**, 75–87.
5 L. M. Bronstein and Z. B. Shifrina, *Chem. Rev.*, 2011, 5301–5344.
6 J. M. Romo-Herrera, R. A. Alvarez-Puebla and L. M. Liz-Marzan, *Nanoscale*, 2011, **3**, 1304–1315.
7 W. Schartl, *Nanoscale*, 2010, **2**, 829–843.
8 M. Murdoch, G. I. N. Waterhouse, M. A. Nadeem, J. B. Metson, M. A. Keane, R. F. Howe, J. Llorca and H. Idriss, *Nat. Chem.*, 2011, **3**, 489–492.
9 M. Haruta, *CATTECH*, 2002, **6**, 102–115.
10 Z. Ma and S. Dai, *ACS Catalysis*, 2011, **1**, 805–818.
11 A. G. Orive, D. Grumelli, C. Vericat, J. M. Ramallo-Lopez, L. Giovanetti, G. Benitez, J. C. Azcarate, G. Corthey, M. H. Fonticelli, F. G. Requejo, A. H. Creus and R. C. Salvarezza, *Nanoscale*, 2011, **3**, 1708–1716.
12 A. Cao, R. Lu and G. Veser, *Phys. Chem. Chem. Phys.*, 2010, **12**, 13499–13510.
13 H. Zhu, Z. Ma, S. Overbury and S. Dai, *Catal. Lett.*, 2007, **116**, 128–135.
14 Q. Zhang, I. Lee, J. Ge, F. Zaera and Y. Yin, *Adv. func. Mat.*, 2010, **20**, 2201–2214.
15 W. Yan, S. M. Mahurin, Z. Pan, S. H. Overbury and S. Dai, *J. Am. Chem. Soc.*, 2005, **127**, 10480–10481.
16 Z. Ma, S. Brown, J. Y. Howe, S. H. Overbury and S. Dai, *Phys.Chem. C*, 2008, **112**, 9448–9457.
17 S. N. Rashkeev, S. Dai and S. H. Overbury, *Phys.Chem. C*, 2010, **114**, 2996–3002.
18 F. Gonzalez de Rivera, L.-I. Rodriguez, O. Rossell, M. Seco, N. J. Divins, I. Casanova and J. Llorca, *J. Organomet. Chem.*, 2011, **696**, 2287–2293.
19 R. P. Vasquez, *SurSS*, 1992, **1**, 129–135.
20 C. D. Wagner, D. E. Passoja, H. F. Hillery, T. G. Kinisky, H. A. Six, W. T. Jansen and J. A. Taylor, *J. Vac. Sci. Technol.*, 1982, **21**, 933–944.
21 P. Buffat and J.-P. Borel, *Phys. Rev. A*, 1976, **13**, 2287–2298.